NONLINEAR CHARACTERISTICS OF SQUARE SOLID-CORE PHOTONIC CRYSTAL FIBERS WITH VARIOUS LATTICE PARAMETERS IN THE CLADDING

Le Tran Bao Tran[a], Dang Van Trong[a], Chu Van Lanh[a], Nguyen Thi Hong Phuong[b], Trang Nguyen Minh Hang[c], Hoang Trong Duc[d], Nguyen Thi Thuy[d*]

[a]Department of Physics, Vinh University, Nghe An, Vietnam
[b]Nguyen Chi Thanh High School, Tay Ninh, Vietnam
[c]IGC Tay Ninh High School, Tay Ninh, Vietnam
[d]The Faculty of Physics, University of Education, Hue University, Thua Thien Hue, Vietnam
[*]Corresponding author: Email: ntthuy@hueuni.edu.vn

Article history
Received: December 4th, 2021
Received in revised form: January 28th, 2022 | Accepted: March 11th, 2022
Available online: October 4th, 2022

Abstract

Nonlinear characteristics of fused silica, solid-core photonic crystal fibers (PCFs) with a square array of air holes are studied numerically. We present a novel design that emphasizes the difference in air hole diameters in the photonic cladding. These PCFs have the advantages of flat dispersion, high nonlinearity, and low attenuation. Based on simulation results, three optimal structures, denoted #F_1, #F_2, and #F_3, having anomalous and all-normal dispersions in the near-infrared range are selected to investigate characteristic properties at the pump wavelength. Such PCFs open up many possibilities for nonlinear optical applications, especially supercontinuum generation.

Keywords: Attenuation; Chromatic dispersion; Different air hole diameters; Nonlinear coefficient; Square photonic crystal fiber.

DOI: https://doi.org/10.37569/DalatUniversity.13.1.1017(2023)

Article type: (peer-reviewed) Full-length research article

1. INTRODUCTION

Many types of research have been conducted on photonic crystal fibers (PCFs), a new type of optical fiber that can be used for a wide range of purposes, such as a transmission medium or in optical devices (Knight et al., 1996; Birks et al., 1997; Russell, 2003; Knight, 2003). Since the first report of their fabrication in 1996, PCFs have received intense attention and are regarded as a breakthrough in fiber optic technology. Commonly, a PCF possesses a central defect region surrounded by a large number of periodically spaced air holes (tubes) running along the length of the fiber. Two types of defects (solid and hollow), with different forms and sizes, act as a core. The propagation of light in a PCF depends on the ratio between the refractive index of the fiber core and the average refractive index of the shell. In the case of solid-core PCFs, because the refractive index of the core is greater than that of the photonic crystal cladding, light is guided by total internal reflection, as with standard fibers (Saitoh & Koshiba, 2005). In contrast, the latter utilize a periodic structure that exhibits a photonic bandgap effect to transmit light in a low index core area. PCFs currently have a very wide spectrum of applications, including use in fiber lasers, light amplifiers, dispersion compensators, and nonlinear processing (Larsen et al., 2003), highly sensitive gas sensors (Jin et al., 2013), polarization sustaining devices, and supercontinuum generation (SCG) (Dinh et al., 2017b; Chu et al., 2019, 2020; Ho & Chu, 2021; Hoang et al., 2019; Zhang et al., 2010).

The outstanding quality of PCF compared to bulk media or conventional fibers is design flexibility through the proper selection of the internal structure, such as the air hole dimensions, lattice shape of the photonic cladding, spacing between two consecutive holes (lattice constant), substrate material, etc. By changing two basic geometrical parameters, the hole diameter (d) and the lattice constant (Λ) (or linear filling factor), it is possible to adjust the dispersion properties, mode shape, transmission spectrum, nonlinearity, and birefringence of the fiber to manage the predicted values. In particular, PCF with a high nonlinear coefficient, flat chromatic dispersion curve, proximity to the zero-dispersion curve, and minimal attenuation is favorable for SCG. However, designing an optical fiber that has all these characteristics is still a considerable challenge for researchers. Many theoretical and experimental studies on the effect of structural parameters on the light-guiding properties of various PCFs have achieved encouraging results, such as ultra-flattened dispersion (Weirich et al., 2010; Gundu et al., 2006), low confinement, high nonlinearity, and birefringence (Arif et al., 2017), ultra-broadband and compactness (Wang et al., 2020), high negative dispersion (Pandey et al., 2020). Among them, the number of studies of PCFs with hexagonal lattices predominates. Moreover, most of the studies cited above use the same diameter parameters for all air hole rings in the coating to simplify future fiber development; thus, dispersion can be optimized but not fiber loss.

In this paper, we use Lumerical MODE Solutions software to design a silica-based solid-core PCF with a square structure in which differences in air hole diameters of the rings are investigated. The optical features are studied by taking into account the influence of the main structural parameters, namely, the filling factor of the first ring (f_1) and the lattice constant (Λ). As a result, three fibers with optimal dispersion (Λ = 0.8 μm, f_1 = 0.55;

Λ = 0.8 µm, f_1 = 0.65; and Λ = 1.0 µm, f_1 = 0.45) are analyzed in detail for effective mode area, nonlinearity, and attenuation characteristics. This new approach is of fundamental importance to the formation of supercontinuum.

2. NUMERICAL MODELING AND SIMULATION RESULTS

As shown schematically in Figure 1a, the PCF structure considered in this study is composed of a solid core and eight air hole rings in a square arrangement. The cladding factor of the linear filling is defined as $f = d/\Lambda$, where d is the diameter of a single air hole and Λ is the lattice constant. We assume that each structure has the same silica glass (SiO_2) as the base material, which helps to induce a large difference in the refractive index of the core and the cladding, causing the light to be strongly restricted to the core (Figure 1b). Saitoh et al. (2003) proved that the dispersion properties of the guided modes, including zero-dispersion wavelength (ZDW), are dominated by the lattice parameters in the first ring near the core, while mode attenuation is dominated by the other rings, particularly for higher modes. Therefore, our idea is to design the first row of holes with diameter d_1 and a filling factor ($f_1 = d_1/\Lambda$) that varies from 0.3 to 0.8 at an increment of 0.05. The linear filling factor of the second and subsequent rings ($f_2 = d_2/\Lambda$) is kept constant at the maximum value of 0.95. The core diameter is calculated by the formula $D_c = 2\Lambda - d_1$, and Λ is taken from 0.7 µm, 0.8 µm, 1.0 µm, and 1.5 µm. Note that it is very difficult to simultaneously control the characteristics of PCFs in previous models (Le et al., 2020; Guo et al., 2021; Dinh et al., 2017b; Hoang et al., 2018; Nguyen et al., 2020; Le et al., 2018) because of their simple structures (i.e., a constant air hole size for all rings). Therefore, creating fibers with optimal chromatic dispersion and extremely small loss is an innovation and a great achievement of our present design. From 44 obtained structures, we chose structures having a flat dispersion for the fundamental mode to calculate the nonlinear optical parameters in the 0.5–2 µm wavelength range.

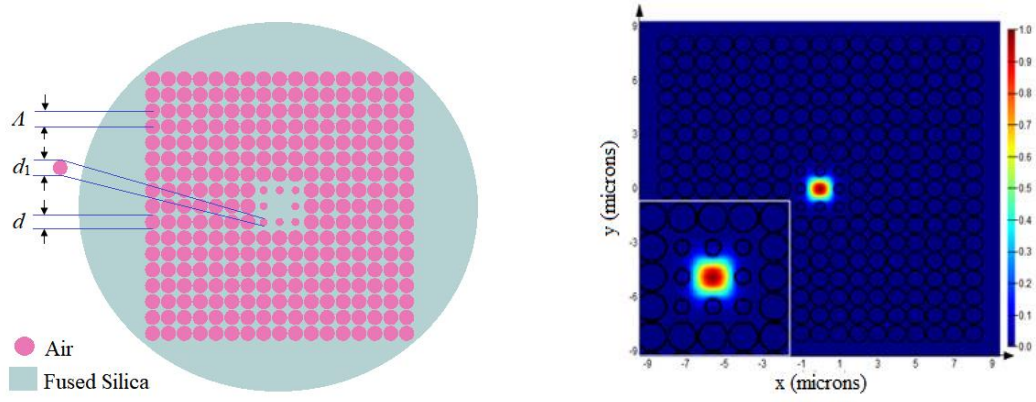

(a) (b)

Figure 1. (a) Geometrical structure diagram; (b) intensity distribution in the PCF with a square array of holes and a silica substrate

Note: The color scale is in relative units.

Numerical analysis was performed using the finite difference eigenmode method, which is commonly employed to treat the optical properties of fibers with complex structures. The analysis used commercial Lumerical MODE Solutions software combined with an anisotropic perfectly matched layer. Chromatic dispersion (D) was obtained as a function of wavelength from the real part of the effective refractive index ($Re[n_{eff}]$) with units of ps·nm^{-1}·km^{-1}, where λ is the wavelength and c represents the speed of light in a vacuum (Saitoh & Koshiba, 2005):

$$D = -\frac{\lambda}{c}\frac{d^2(\mathrm{Re}[n_{eff}]}{d\lambda^2}. \quad (1)$$

By inputting the scanning electron microscopy image of the real fiber, we applied the refractive index distribution of the fused silica glass in the numerical simulations, which takes account of all imperfections that occurred during the evolution. The wavelength-dependent refractive index can be described using Sellmeier's equation (Equation 2) (Stepniewski et al., 2016; Kedenburg et al., 2012):

$$n^2(\lambda) = B_0 + \frac{B_1\lambda^2}{\lambda^2 - C_1} + \frac{B_2\lambda^2}{\lambda^2 - C_2} + \frac{B_3\lambda^2}{\lambda^2 - C_3} \quad (2)$$

with the coefficients B_0 = 1, B_1 = 0.6694226, B_2 = 0.4345839, B_3 = 0.8716947, C_1 = 4.4801×10^{-3} μm^2, C_2 = 1.3285×10^{-2} μm^2, and C_3 = 95.341482 μm^2. The refractive index of air is assumed to be 1 for all wavelengths.

To investigate the impact of structural parameters on the PCF properties, we first compare the effective refractive index for the fundamental mode in the wavelength region λ = 0.5–2 μm in Figure 2. As observed, the mode refractive indices decrease with increasing wavelength and have a similar shape in all cases. This behavior is mostly because longer wavelengths have a stronger ability to penetrate within the cladding portion of the PCF than shorter wavelengths (Dhara & Singh, 2021). On the other hand, the variation of the effective refractive index characteristic is also greatly influenced by two lattice parameters, Λ and f_1. It can be seen that the n_{eff} curves rise for the structures with a larger lattice constant and conversely. In particular, for the low filling factor f_1 = 0.3, we obtained higher values and a smaller slope for n_{eff} than in the case of f_1 = 0.8, owing to the enlargement of the core and the greater contribution of fused silica to the cladding refractive index (Chu et al., 2017).

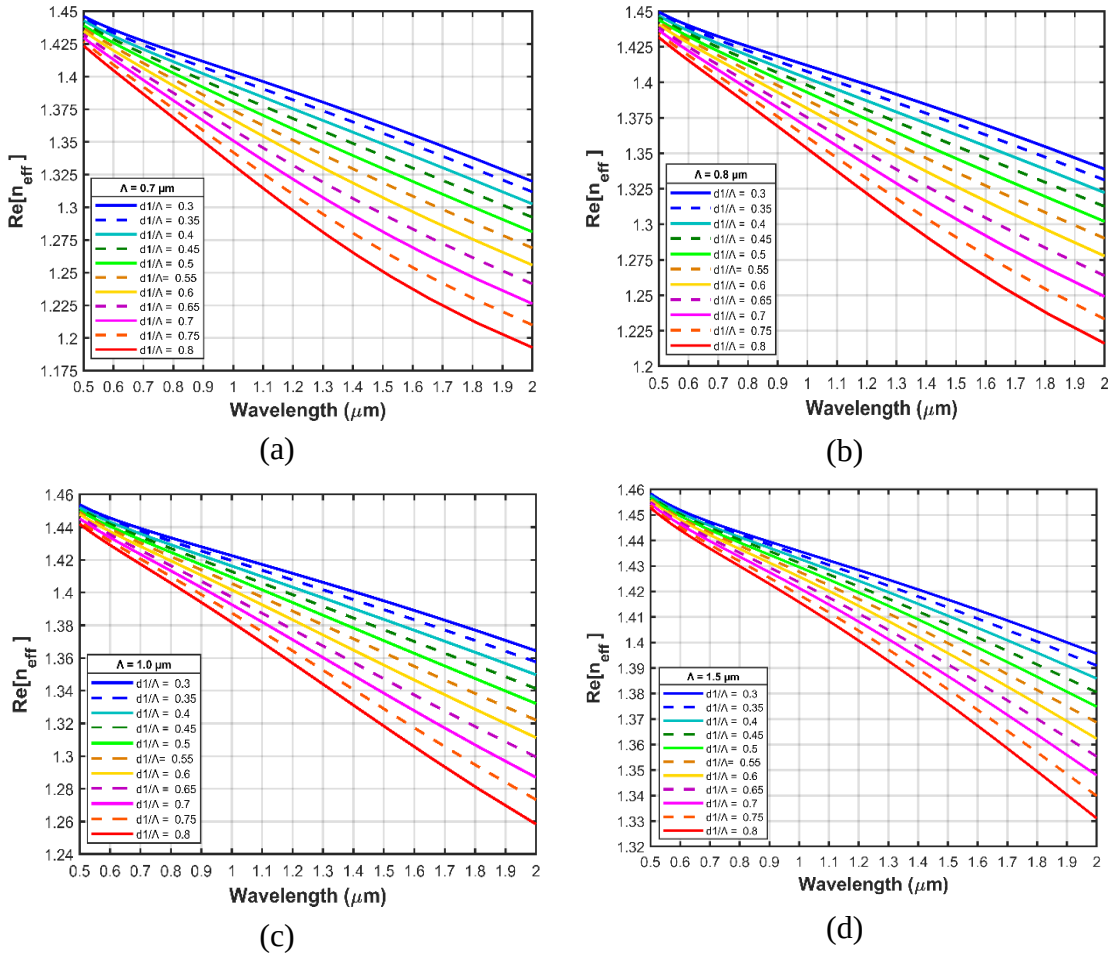

Figure 2. The real part of the effective refractive indices versus wavelength for the PCFs with f_1 = 0.3–0.8 and various lattice constants: (a) Λ = 0.7 µm; (b) Λ = 0.8 µm; (c) Λ = 1.0 µm; (d) Λ = 1.5 µm

Figure 3 illustrates the relationship between dispersion and wavelength for different values of Λ and f_1 for all structural groups. Overall, it is clear that the alteration of lattice constant and filling factor dramatically modifies the position of dispersion; the shape of the dispersion curves corresponding to lattice constants is similar except for Λ = 1.5 µm. The variety of dispersion characteristics is seen in the case of a small core (Λ = 0.7 and 0.8 µm) involving all-normal and anomalous states together with the existence of a zero-dispersion wavelength because of the dominance of waveguide dispersion (Rostami & Soofi, 2011). However, almost all of these curves are highly sloped and less flat, principally in the short wavelength region. This is explained by the dependence of dispersion on the effective refractive index and wavelength according to Equation (1). By increasing the PCF lattice constant, the flattened dispersion window is enhanced and the sign of dispersion is changed from negative to positive. Specifically, all large-core fibers exhibited anomalous dispersion in the range $\lambda > 0.7$ µm with most PCFs possessing one ZDW (Figures 3c and 3d).

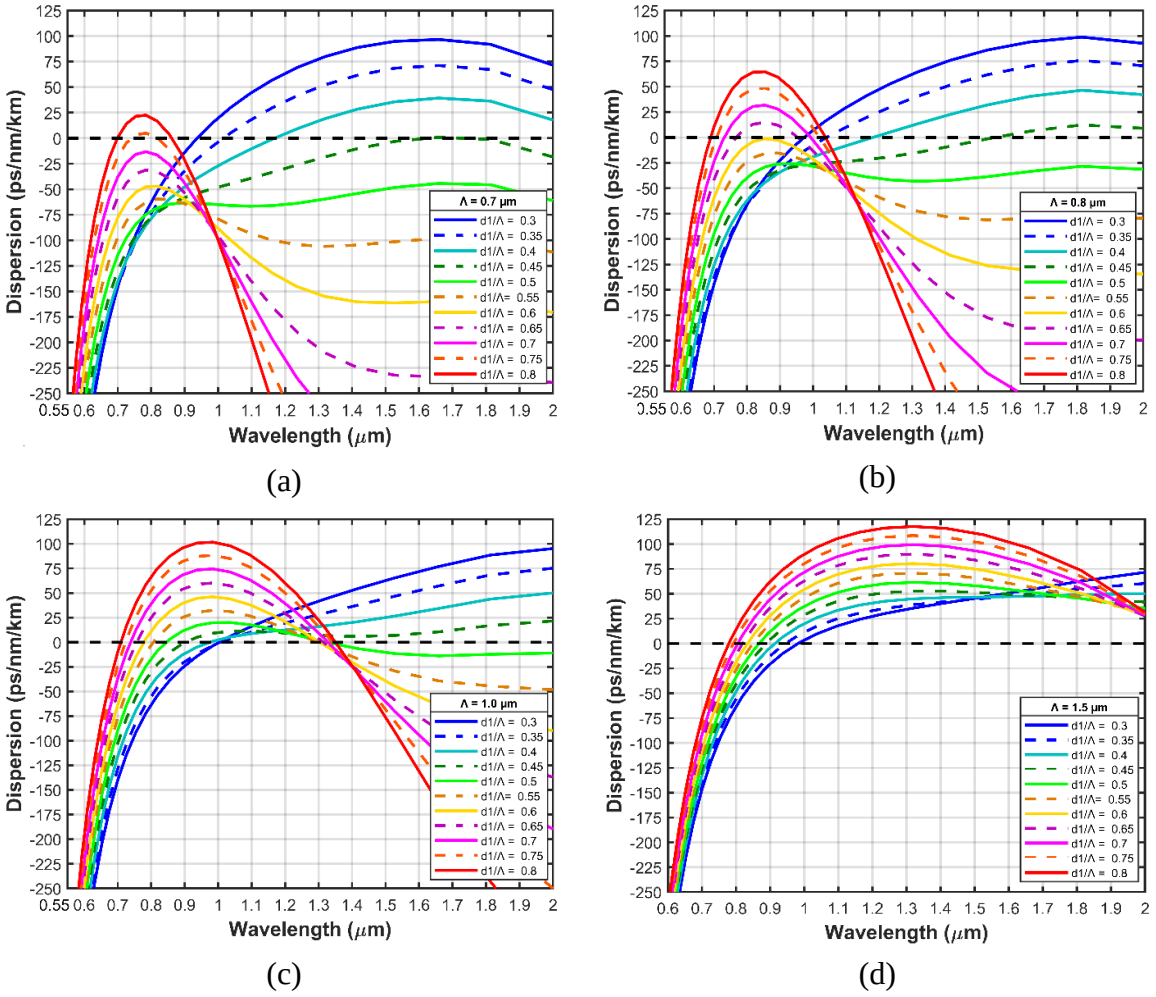

Figure 3. Characteristics of the chromatic dispersion of the proposed fibers for f_1 = 0.3–0.8 and various lattice constants: (a) Λ = 0.7 μm; (b) Λ = 0.8 μm; (c) Λ = 1.0 μm; (d) Λ = 1.5 μm

Note: The black dashed line denotes zero dispersion.

The numerical results depicted in Figure 3 also show a huge variation in the dispersion profile with the change in filling factor. The small-core fibers have dispersions with one ZDW at low filling factor values (f_1 < 0.5), and they tend to be completely located in the normal dispersion when f_1 rises to 0.7. In contrast, the dispersion curves of the fibers with large f_1 values intersect the zero-dispersion line at two points, that is, dispersions with two ZDWs are achieved in the wavelength zone of interest (Figure 3a). Additionally, for a given value of Λ, higher filling factors in the first ring result in blueshifts of ZDW_1, whereas ZDW_2 shifts toward longer wavelengths. As the core diameter is further enlarged (Λ = 1.5 μm), ZDWs are usually moderately shifted to the long-wavelength range with falling f_1. Obviously, the versatile modification of the lattice structure in our design dramatically influences the confinement of light in the core. Thus, the geometric parameters are important factors in tuning the dispersion feature. In particular, the acquisition of the all-normal dispersion regime is extremely interesting and

meaningful for the highly coherent and flat-top SCG spectral broadening through the support of two typical mechanisms, self-phase modulation and optical wave-breaking, which could not be attained in several other studies (Le et al., 2020; Hoang et al., 2018; Nguyen et al., 2020; Le et al., 2018; Pniewski et al., 2016).

3. ANALYSIS OF OPTICAL PROPERTIES OF OPTIMIZED PCF

The dispersion parameter is one of the substantial properties for nonlinear optical applications, and at the same time, it plays a key role in the propagation of short optical pulses with different wavelength and speed components in the medium. The flat all-normal, near-zero dispersion curves and the compatibility of ZDW with the pump wavelength are the determining factors for generating an ultra-broadband supercontinuum. Therefore, the goal of dispersion optimization here is to identify fiber structures satisfying the above features and to analyze and evaluate their suitability in SCG applications. Based on preliminary calculations, we propose three PCFs (labeled #F_1, #F_2, and #F_3) with the structural parameters shown in Table 1. The suggested fibers, having diverse dispersions, may be suitable for generating noncoherent and coherent supercontinua corresponding to the appropriate input pulse. The dispersion characteristics of the fundamental mode for these three fibers are displayed in Figure 4. The first structure, #F_1, has an interesting dispersion profile with a positive slope and comes closest to the zero-dispersion line, with a ZDW at about 0.903 μm and a flat plateau of anomalous dispersion that extends from about 1000 nm. The dispersion value is equal to 10.898 ps·nm^{-1}·km^{-1} at the central wavelength of the input pulse (pump wavelength) of 1.03 μm. Structure #F_2 exhibits all-normal dispersion over the considered near-infrared range and is expected to pump at 0.85 μm; its dispersion is −16.294 ps·nm^{-1}·km^{-1}. In the wavelength range of 0.7–0.89 μm, its dispersion varies from −77 to −15 ps·nm^{-1}·km^{-1} and is flatter in the long wavelength region. The same phenomenon can be perceived in the fibers with Λ = 0.7 μm. Nevertheless, in the long-wavelength region, these PCFs diminish the spectral broadening and brightness of SCG because their core diameter is smaller than that of the #F_2 fiber, and they cause a high confinement loss in that zone (Le et al., 2018). The #F_3 fiber exhibits dispersion with two ZDWs, at 0.768 μm (ZDW_1) and 0.953 μm (ZDW_2), and a dispersion value of 14.676 ps·nm^{-1}·km^{-1} at the same pump wavelength as the second fiber. Thus, the #F_2 fiber can be used for broad all-normal dispersion SCG, whereas SCG based on soliton separation should be performed by others.

Table 1. Geometrical parameters of the proposed PCFs

#	Λ (μm)	f_1	D_c (μm)
#F_1	1.0	0.45	1.55
#F_2	0.8	0.55	1.16
#F_3	0.8	0.65	1.08

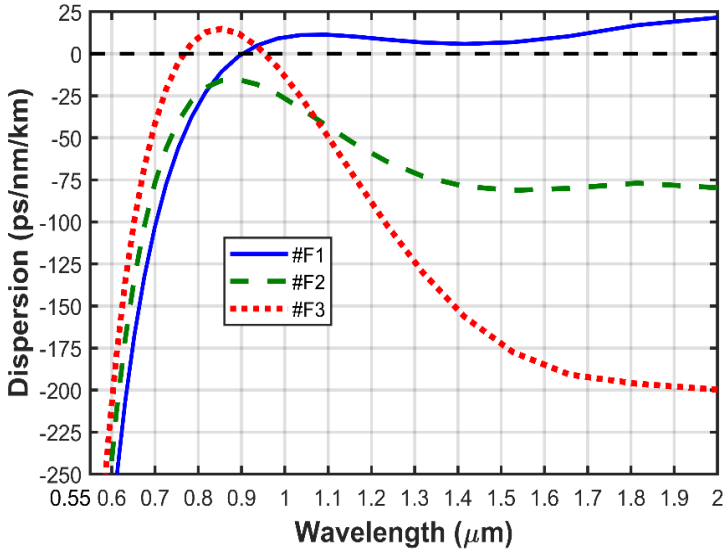

Figure 4. Dispersion profiles of the fundamental mode for the structures #F_1 (solid line), #F_2 (dashed line), and #F_3 (dotted line)

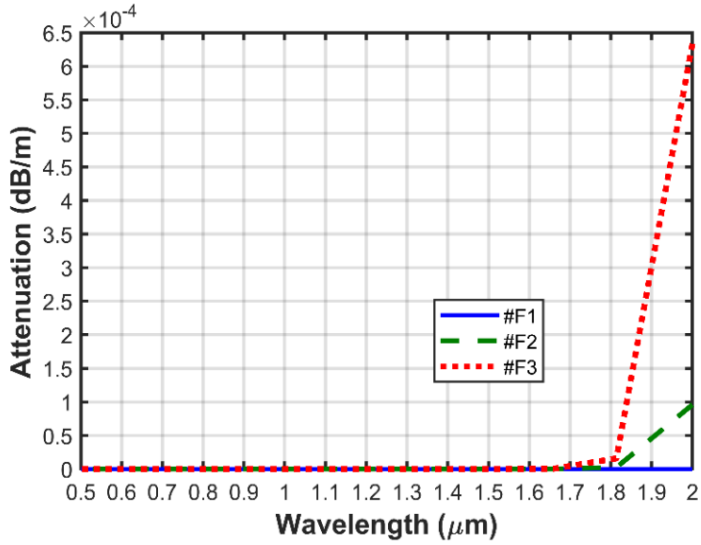

Figure 5. Attenuation properties of the three optimal PCFs

The attenuation of the examined PCFs is determined by the material and the waveguide confinement loss. As the modes are well confined in the core and the majority of the electromagnetic field is located there, they mainly follow the material loss of silica. Figure 5 specifies the attenuation characteristics (L_k) as a function of the wavelength for the proposed structures. The difference in the values of all three PCFs is negligible in the 0.5 to 1.7 μm wavelength region. The #F_1 fiber reveals the smallest attenuation in the whole surveyed wavelength range; this curve is almost coincident with the horizontal axis. In particular, when the wavelengths are greater than 1.7 μm, the attenuation of the #F_3 fiber grows abruptly to reach a maximum of about 0.00064 dB/m at λ = 2 μm while that of #F_2 is much lower. One reason for this is that the #F_3 fiber has a small core diameter

compared to wavelengths in this range; therefore, it is possible to predict that $\#F_3$ does not support the guide mode inside the core at the long wavelengths. For the given central wavelength of the pump source, the L_k values are -2.873×10^{-19} dB/m, 1.969×10^{-20} dB/m and -1.221×10^{-18} dB/m for $\#F_1$, $\#F_2$, and $\#F_3$, respectively. The low attenuation is a prominent feature of our model. Careful consideration of the various air hole ring diameters has offered a solution to the limitations of previous efforts (Hoang et al., 2018; Pniewski et al., 2016), namely, the simultaneous optimization of the loss and chromatic dispersion of PCFs.

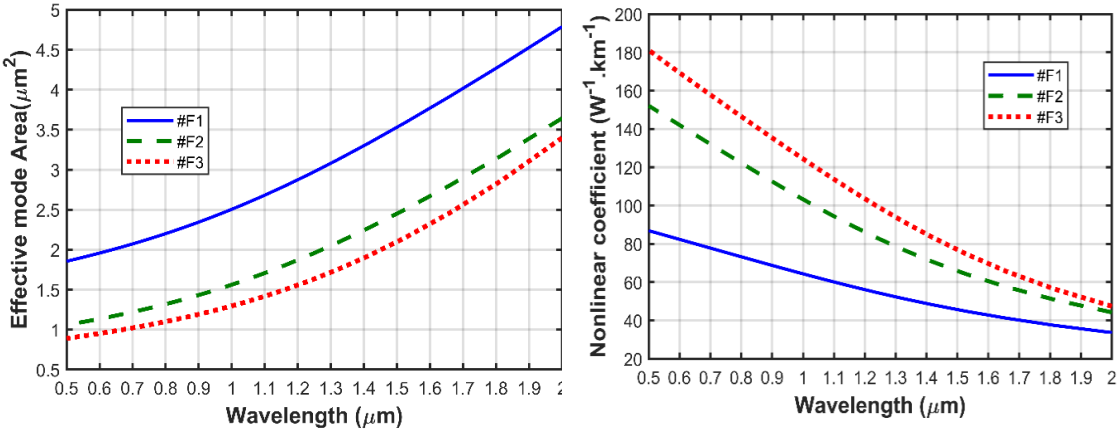

(a) (b)

Figure 6. (a) Effective mode area; (b) nonlinear coefficient of three optimal PCFs

Table 2. Characteristic properties of the proposed PCFs calculated at the pump wavelength

#	The pump wavelength (μm)	D ($ps\cdot nm^{-1}\cdot km^{-1}$)	A_{eff} (μm^2)	γ ($W^{-1}\cdot km^{-1}$)	L_k (dB/m)
$\#F_1$	1.03	10.898	2.555	63.065	-2.873×10^{-19}
$\#F_2$	0.85	−16.294	1.373	117.366	1.969×10^{-20}
$\#F_3$	0.85	14.676	1.144	140.892	-1.221×10^{-18}

Figure 6 presents the effective mode area (A_{eff}) and nonlinear coefficient (γ) of the fundamental mode for the selected PCFs. The graphs show that the optical properties of the $\#F_2$ and $\#F_3$ fibers are similar, but they are remarkably different from $\#F_1$ over all wavelengths. It can be observed that the A_{eff} curves rise rather linearly with increasing wavelength (Figure 6a). With the large core diameters, the $\#F_1$ fiber has the highest effective mode area and the $\#F_3$ fiber has the lowest among the structures at all wavelengths. Consequently, the nonlinear coefficient of the PCFs has the opposite tendency; it falls with an increase in wavelength since it is inversely proportional to A_{eff} according to the formula $\gamma = 2\pi n_2/\lambda A_{eff}$ (Agrawal, 2013). A larger effective mode area means lower energy density and hence weaker nonlinear effects. As a result, the $\#F_3$ minor core fiber with the smallest effective mode area has the greatest nonlinearity in the investigated wavelength region. High nonlinear PCF is the most desirable for

supercontinuum generation with low input energies, such as picojoules. With the same pumped wavelength of 0.85 μm, the nonlinear coefficients of the $\#F_2$ and $\#F_3$ structures equal 117.366 $W^{-1}\cdot km^{-1}$ and 140.892 $W^{-1}\cdot km^{-1}$, respectively, whereas this value is 63.065 $W^{-1}\cdot km^{-1}$ at the wavelength of 1.03 μm for $\#F_1$. These numbers are much greater than the nonlinearity reported for solid-core PCFs in other studies (Hoang et al., 2018; Le et al., 2018). The effective mode areas for the three fibers, $\#F_1$, $\#F_2$, and $\#F_3$, are 2.555 μm^2, 1.373 μm^2, and 1.144 μm^2, respectively. The optical properties of the proposed PCFs computed at the pump wavelength are given in Table 2. In summary, the results demonstrate that these PCFs are quite appropriate for SCG applications.

4. CONCLUSION

A new technique that uses different geometric structures to control the characteristic properties of fused silica PCF is discussed. By varying the lattice constant and the filling factor of the first ring near the core, these PCFs provide efficient dispersion controllability to tune the zero-dispersion wavelengths and change the sign of the dispersion over a broad spectral range. We have chosen three fiber structures with flat all-normal and anomalous dispersions (Λ = 1.0 μm, f_1 = 0.45; Λ = 0.8 μm, f_1 = 0.55 and 0.65) to additionally conduct the modal analysis in terms of effective mode area, nonlinear coefficient, and loss of the fundamental mode. Our simulation results are valuable for using the suggested PCFs for supercontinuum generation because of their optimal dispersion, high nonlinearity, and low attenuation.

ACKNOWLEDGMENTS

This research is funded by the Vietnam National Foundation for Science and Technology Development (NAFOSTED) under grant number 103.03-2020.03 and the Vietnam Ministry of Education and Training (B2021-DHH-08).

REFERENCES

Agrawal, G. (2013). Highly nonlinear fibers. In *Nonlinear fiber optics* (5th ed.) (pp. 457-496). Elsevier. https://doi.org/10.1016/B978-0-12-397023-7.00011-5

Arif, M. F. H., Biddut, M. J. H., Babu, M. S. I., Rahman, H. M. M., Rahman, M. M., Jahan, B., Chaity, M. S., & Khaled, S. M. (2017). Photonic crystal fiber based sensor for detecting binary liquid mixture. *Optics and Photonics Journal*, *7*(11), 221-234. https://doi.org/10.4236/opj.2017.711020

Birks, T. A., Knight, J. C., & Russell, P. St. J. (1997). Endlessly single-mode photonic crystal fiber. *Optics Letters*, *22*(13), 961-963. https://doi.org/10.1364/OL.22.000961

Chu, V. L., Anuszkiewicz, A., Ramaniuk, A., Kasztelanic, R., Dinh, X. K., Cao, L. V., Trippenbach, M., & Buczyński, R. (2017). Supercontinuum generation in photonic crystal fibres with core filled with toluene. *Journal of Optics*, *19*(12), 125604. https://doi.org/10.1088/2040-8986/aa96bc

Chu, V. L., Hoang, V. T., Cao, L. V., Borzycki, K., Dinh, X. K., Tran, Q. V., Trippenbach, M., Buczyński, R., & Pniewski, J. (2019). Optimization of optical properties of photonic crystal fibers infiltrated with chloroform for supercontinuum generation. *Laser Physics*, *29*(7), 075107. https://doi.org/10.1088/1555-6611/ab2115

Chu, V. L., Hoang, V. T., Cao, L. V., Borzycki, K., Dinh, X. K., Tran, Q. V., Trippenbach, M., Buczyński, R., & Pniewski, J. (2020). Supercontinuum generation in photonic crystal fibers infiltrated with nitrobenzene. *Laser Physics*, *30*(3), 035105. https://doi.org/10.1088/1555-6611/ab6f09

Dhara, P., & Singh, V. K. (2021). Investigation of rectangular solid-core photonic crystal fiber as temperature sensor. *Microsystem Technologies*, *27*, 127-132. https://doi.org/10.1007/s00542-020-04927-1

Dinh, X. K., Chu, V. L., Cao, L. V., Ho, D. Q., Mai, V. L., Trippenbach, M., & Buczyński, R. (2017a). Influence of temperature on dispersion properties of photonic crystal fibers infiltrated with water. *Optical and Quantum Electronics*, *49*(2), 87. https://doi.org/10.1007/s11082-017-0929-3

Dinh, X. K., Chu, V. L., Ho, D. Q., Luu, V. X., Trippenbach, M., & Buczynski, R. (2017b). Dispersion characteristics of a suspended-core optical fiber infiltrated with water. *Applied Optics*, *56*(4), 1012-1019. https://doi.org/10.1364/AO.56.001012

Gundu, K. M., Kolesik, M., Moloney, J. V., & Lee, K. S. (2006). Ultra-flattened-dispersion selectively liquid-filled photonic crystal fibers. *Optics Express*, *14*(15), 6870-6878. https://doi.org/10.1364/OE.14.006870

Guo, Y., Yuan, J., Wang, K., Wang, H., Cheng, Y., Zhou, X., Yan, B., Sang, X., & Yu, C. (2021). Generation of supercontinuum and frequency comb in a nitrobenzene-core photonic crystal fiber with all-normal dispersion profile. *Optics Communications*, *481*(4), 126555. https://doi.org/10.1016/j.optcom.2020.126555

Ho, Q. Q., & Chu, V. L. (2021). Spectrum broadening of supercontinuum generation by fill styrene in core of photonic crystal fibers. *Indian Journal of Pure & Applied Physics*, *59*, 522-527.

Hoang, V. T., Kasztelanic, R., Filipkowski, A., Stępniewski, G., Pysz, D., Klimczak, M., Ertman, S., Cao, L. V., Woliński, T. R., Trippenbach, M., Dinh, X. K., Śmietana, M., & Buczyński, R. (2019). Supercontinuum generation in an all-normal dispersion large core photonic crystal fiber infiltrated with carbon tetrachloride. *Optical Materials Express*, *9*(5), 2264-2278. https://doi.org/10.1364/OME.9.002264

Hoang, V. T., Siwicki, B., Franczyk, M., Stępniewski, G., Le, V. H., Cao, L. V., Klimczak, M., & Buczyński, R. (2018). Broadband low-dispersion low-nonlinearity photonic crystal fiber dedicated to near-infrared high-power femtosecond pulse delivery. *Optical Fiber Technology*, *42*, 119-125. https://doi.org/10.1016/j.yofte.2018.03.003

Jin, W., Ju, J., Ho, H. L., Hoo, Y. L., & Zhang, A. (2013). Photonic crystal fibers, devices, and applications. *Frontiers of Optoelectronics*, *6*(1), 3-24. https://doi.org/10.1007/s12200-012-0301-y

Kedenburg, S., Vieweg, M., Gissibl, T., & Giessen, H. (2012). Linear refractive index and absorption measurements of nonlinear optical liquids in the visible and near-infrared spectral region. *Optical Materials Express*, *2*(11), 1588-1611. https://doi.org/10.1364/OME.2.001588

Knight, J. C. (2003). Photonic crystal fibres. *Nature*, *424*(6950), 847-851. https://doi.org/10.1038/nature01940

Knight, J. C., Birks, T. A., Russell, P. St. J., & Atkin, D. M. (1996). All-silica single-mode optical fiber with photonic crystal cladding. *Optics Letters*, *21*(19), 1547-1549. https://doi.org/10.1364/OL.21.001547

Larsen, T. T, Bjarklev, A., Hermann, D. S., & Broeng, J. (2003). Optical devices based on liquid crystal photonic bandgap fibres. *Optics Express*, *11*(20), 2589-2596. https://doi.org/10.1364/OE.11.002589

Le, T. B. T., Nguyen, T. T., Vo, T. M. N., Le, C. T., Le, V. M., Cao, L. V., Dinh, X. K., & Chu, V. L. (2020). Analysis of dispersion characteristics of solid-core PCFs with different types of lattice in the claddings, infiltrated with ethanol. *Photonics Letters of Poland*, *12*(4), 106-108. https://doi.org/10.4302/plp.v12i4.1054

Le, V. H., Cao, L. V., Nguyen, T. H., Nguyen, M. A., Buczyński, R., & Kasztelanic, R. (2018). Application of ethanol infiltration for ultra-flattened normal dispersion in fused silica photonic crystal fibers. *Laser Physics*, *28*(11), 115106. https://doi.org/10.1088/1555-6611/aad93a

Nguyen, T. T., Chu, T. G. T., Le, V. M., Tran, Q. V., Doan, Q. K, Dinh, X. K., Chu, V. L., & Le, T. B. T. (2020). Numerical analysis of the characteristics of glass photonic crystal fibers infiltrated with alcoholic liquids. *Communications in Physics*, *30*(3), 209-220. https://doi.org/10.15625/0868-3166/30/3/14815

Pandey, S. K., Prajapati, Y. K., & Maurya, J. B. (2020). Design of simple circular photonic crystal fiber having high negative dispersion and ultra-low confinement loss. *Results in Optics*, *1*, 100024. https://doi.org/10.1016/j.rio.2020.100024

Pniewski, J., Stefaniuk, T., Le, V. H., Cao, L. V., Chu, V. L., Kasztelanic, R., Stępniewski, G., Ramaniuk, A., Trippenbach, M., & Buczyński, R. (2016). Dispersion engineering in nonlinear soft glass photonic crystal fibers infiltrated with liquids. *Applied Optics*, *55*(19), 5033-5040. https://doi.org/10.1364/AO.55.005033

Rostami, A., & Soofi, H. (2011). Correspondence between effective mode area and dispersion variations in defected core photonic crystal fibers. *Journal of Lightwave Technology*, *29*(2), 234-241. https://doi.org/10.1109/JLT.2010.2100808

Russell, P. St. J. (2003). Photonic crystal fibers. *Science*, *299*(5605), 358-362. https://doi.org/10.1126/science.1079280

Saitoh, K., & Koshiba, M., (2005). Numerical modeling of photonic crystal fibers. *Journal of Lightwave Technology*, *23*(11), 3580-3590. https://doi.org/10.1109/JLT.2005.855855

Saitoh, K., Koshiba, M., Hasegawa, T., & Sasaoka, E. (2003). Chromatic dispersion control in photonic crystal fibers: Application to ultra-flattened dispersion. *Optics Express*, *11*(8), 843-852. https://doi.org/10.1364/OE.11.000843

Stepniewski, G., Kasztelanic, R., Pysz, D., Stepien, R., Klimczak, M., & Buczynski, R. (2016). Temperature sensitivity of chromatic dispersion in nonlinear silica and heavy metal oxide glass photonic crystal fibers. *Optical Materials Express*, *6*(8), 2689-2703. https://doi.org/10.1364/OME.6.002689

Wang, Y., Li, S., Wu, J., Yu, P., & Li, Z. (2020). Design of an ultrabroadband and compact filter based on square-lattice photonic crystal fiber with two large gold-coated air holes. *Photonics and Nanostructures-Fundamentals and Applications*, *41*, 100816. https://doi.org/10.1016/j.photonics.2020.100816

Weirich, J., Lægsgaard, J., Wei, L., Alkeskjold, T. T., Wu, T. X., Wu, S-T., & Bjarklev, A. O. (2010). Liquid crystal parameter analysis for tunable photonic bandgap fiber devices. *Optics Express*, *18*(5), 4074-4087. https://doi.org/10.1364/OE.18.004074

Zhang, H., Chang, S., Yuan, J., & Huang, D. (2010). Supercontinuum generation in chloroform-filled photonic crystal fibers. *Optik*, *121*(9), 783-787. https://doi.org /10.1016/j.ijleo.2008.09.026